Coherence effects in digital in-line holographic microscopy

Unnikrishnan Gopinathan,* Giancarlo Pedrini, and Wolfgang Osten

Institut für Technische Optik, Universitäat Stuttgart, Pfaffenwaldering 9, 70569 Stuttgart, Germany
**Corresponding author: unni.gopinathan@gmail.com*

Received June 12, 2008; accepted July 21, 2008;
posted August 12, 2008 (Doc. ID 97336); published September 17, 2008

We analyze the effects of partial coherence in the image formation of a digital in-line holographic microscope (DIHM). The impulse response is described as a function of cross-spectral density of the light used in the space-frequency domain. Numerical simulation based on the applied model shows that a reduction in coherence of light leads to broadening of the impulse response. This is also validated by results from experiments wherein a DIHM is used to image latex beads using light with different spatial and temporal coherence. © 2008 Optical Society of America

OCIS codes: 030.1640, 030.1670, 030.4070, 090.1995, 170.0180.

1. INTRODUCTION

In-line holography with spherical waves using a lensless configuration was originally proposed by Gabor [1] while attempting to address the problem of lens aberrations in electron microscopy. To address the practical issues associated with the hologram reconstruction in the original method, one of the approaches was to record the hologram digitally and use numerical techniques for reconstruction. These methods have been generically referred to as digital in-line holography (DIH) [2]. Many novel recording and reconstruction methods have been proposed to extract information regarding three-dimensional complex amplitude distribution [3–5] uncorrupted by twin image and three-dimensional complex spatial coherence distribution [6].

Over the years, DIH has been successfully applied to imaging microscopic objects with electrons [7,8] and photons [9–14]. Most of these works use configurations without a lens. In addition to eliminating aberrations, the lensless configuration is well suited for a wide range of sources including x rays and deep ultraviolet for improved resolution [15–17].

In many applications using DIH, it is common to treat the source as completely coherent, both spatially and temporally. This assumption, though valid in many cases, will not hold for all. For instance, x-ray sources are partially coherent. Partially coherent light is also used for many applications in optical microscopy [18–20]. These applications would benefit from a generalized treatment that takes into account the state of coherence of light. Effects of spatial coherence in lensless Fresnel holography [21,22] and in-line Gabor holography [23] have been studied earlier. However these works have mainly dealt with the spatial coherence effects for the case of quasi-monochromatic light.

In this paper we provide a theoretical framework for analyzing the partial coherence effects in the image formation of a digital in-line holographic microscope (DIHM). The analysis presented is valid for primary or secondary sources of any state of coherence. The state of coherence of the source is characterized by the cross-spectral density (CSD) [24–26] in the space-frequency domain. The analysis in the space-frequency domain allows us to account for any dispersive effect of the object. We provide an expression for the impulse response in terms of CSD of the source. The impulse response for the case of a Gaussian Schell source is simulated. It is seen that a reduction in coherence of the light leads to broadening of the impulse response. This is also validated by results from experiments wherein a DIHM is used to image latex beads using light with different spatial and temporal coherence.

2. IMPULSE RESPONSE FOR PARTIALLY COHERENT LIGHT

A. Hologram Formation

The geometry of the system discussed is shown in Fig. 1. Let σ denote the illumination pupil of a planar secondary source illuminated by a primary source directly or indirectly (through an optical system) with a coherence state characterized by the CSD function $W(\mathbf{p_1},\mathbf{p_2},\omega)$ of the fluctuating field $U(\mathbf{p_1},\mathbf{t})$ and $U(\mathbf{p_2},\mathbf{t})$ at two points P_1 and P_2 in the secondary source illumination pupil σ; $\mathbf{p_1}$ and $\mathbf{p_2}$ are the position vectors of two points P_1 and P_2. If the fluctuations $U(\mathbf{p_1},\mathbf{t})$ and $U(\mathbf{p_2},\mathbf{t})$ are members of the statistical ensemble $\{U(\mathbf{p},t)=U(\mathbf{p},\omega)e^{-j\omega t}\}$ that is stationary at least in the wide sense, Wolf [26] has shown that $W(\mathbf{p_1},\mathbf{p_2},\omega)$ may be expressed as a correlation function in the space-frequency domain as

$$W(\mathbf{p_1},\mathbf{p_2},\omega)=\langle U^*(\mathbf{p_1},\omega)U(\mathbf{p_2},\omega)\rangle_\omega. \tag{1}$$

To find out the impulse response of the system, we consider the interference between the light emanating from the source and the light scattered from a point object located at the point Q with a position vector $\mathbf{r_i}$. The scat-

 © 2008 Optical Society of America

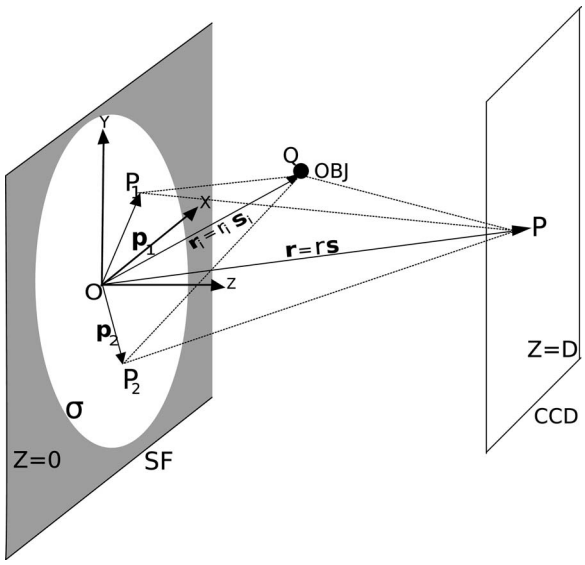

Fig. 1. Schematic illustrating the notations used in the text. SF denotes spatial filter (see Fig. 4).

tered wave from the object may be considered to be a spherical wave emanating from the point Q with an amplitude $\Theta(\mathbf{r_i},\omega)$. The scattered and unscattered component of the light from the point P_1 reaches the point P following two paths P_1QP and P_1P given by

$$V_1(\mathbf{r},\omega)=\Theta(\mathbf{r_i},\omega)U(\mathbf{p_1},\omega)\frac{e^{jk|\mathbf{r_i}-\mathbf{p_1}|}}{|\mathbf{r_i}-\mathbf{p_1}|}\frac{e^{jk|\mathbf{r}-\mathbf{r_i}|}}{|\mathbf{r}-\mathbf{r_i}|}+U(\mathbf{p_1},\omega)\frac{e^{jk|\mathbf{r}-\mathbf{p_1}|}}{|\mathbf{r}-\mathbf{p_1}|}. \tag{2}$$

If the distance of the scatterer r_i from the source is quite large compared to the source dimension, the term $|\mathbf{r_i}-\mathbf{p_1}|$ may be approximated as $r_i-\mathbf{s_i}\cdot\mathbf{p_1}$ in the numerator and as r_i in the denominator; $\mathbf{s_i}$ is the unit vector along the vector $\mathbf{r_i}$. In the numerator, $|\mathbf{r_i}-\mathbf{p_1}|$ appears in the exponential term multiplied by the factor k. Hence, the approximation to $|\mathbf{r_i}-\mathbf{p_1}|$ used is different in the numerator and the denominator. Similarly, if the point P lies sufficiently far away from the source, the terms $|\mathbf{r}-\mathbf{r_i}|$ and $|\mathbf{r}-\mathbf{p_1}|$ may be approximated as $r-\mathbf{s}\cdot\mathbf{r_i}$ and $r-\mathbf{s}\cdot\mathbf{p_1}$ in the numerator and as r in the denominator, respectively; $\mathbf{s}$ is the unit vector along the vector $\mathbf{r}$. Using the far field approximations given above we may write Eq. (2) as

$$V_1(r\mathbf{s},\omega)=\Theta(\mathbf{r_i},\omega)U(\mathbf{p_1},\omega)\frac{e^{jkr_i}}{r_i}\frac{e^{jkr}}{r}e^{-jk(\mathbf{s_i}\cdot\mathbf{p_1}+\mathbf{s}\cdot\mathbf{r_i})}+U(\mathbf{p_1},\omega)\frac{e^{jkr}}{r}e^{-jk\mathbf{s}\cdot\mathbf{p_1}}. \tag{3}$$

A similar expression may be written for the light from the point P_2 reaching the point P following two paths P_2QP and P_2P given by

$$V_2(r\mathbf{s},\omega)=\Theta(\mathbf{r_i},\omega)U(\mathbf{p_2},\omega)\frac{e^{jkr_i}}{r_i}\frac{e^{jkr}}{r}e^{-jk(\mathbf{s_i}\cdot\mathbf{p_2}+\mathbf{s}\cdot\mathbf{r_i})}+U(\mathbf{p_2},\omega)\frac{e^{jkr}}{r}e^{-jk\mathbf{s}\cdot\mathbf{p_2}}. \tag{4}$$

The spectral density at the point P is given by

$$S(r\mathbf{s},\omega)=\int_\sigma\int_\sigma\langle V_1^*(r\mathbf{s},\omega)V_2(r\mathbf{s},\omega)\rangle \mathrm{d}^2p_1\mathrm{d}^2p_2. \tag{5}$$

The integration in Eq. (5) is over the source domain σ. All integrals in the following discussion unless otherwise stated run from $-\infty$ to $+\infty$. Substituting Eqs. (3)–(5) we obtain

$$S(\mathbf{s},\omega)=\int_\sigma\int_\sigma W(\mathbf{p_1},\mathbf{p_2},\omega)\left[\frac{|\Theta(\mathbf{r_i},\omega)|^2}{r_i^2}e^{-jk\mathbf{s_i}\cdot(\mathbf{p_2}-\mathbf{p_1})}+e^{-jk\mathbf{s}\cdot(\mathbf{p_2}-\mathbf{p_1})}+\frac{e^{jkr_i}}{r_i}\Theta(\mathbf{r_i},\omega)e^{-jk(\mathbf{s_i}\cdot\mathbf{p_2}+\mathbf{s}\cdot\mathbf{r_i}-\mathbf{s}\cdot\mathbf{p_1})}+\frac{e^{-jkr_i}}{r_i}\Theta^*(\mathbf{r_i},\omega)e^{jk(\mathbf{s_i}\cdot\mathbf{p_1}+\mathbf{s}\cdot\mathbf{r_i}-\mathbf{s}\cdot\mathbf{p_2})}\right]\mathrm{d}^2p_1\mathrm{d}^2p_2. \tag{6}$$

If we interchange $\mathbf{p_1}$ and $\mathbf{p_2}$ in the fourth term and use the relation $W(\mathbf{p_2},\mathbf{p_1},\omega)=W^*(\mathbf{p_1},\mathbf{p_2},\omega)$ (valid for any CSD function [24,25]), it may be noted that the fourth term in Eq. (6) is the complex conjugate of the third term. It may be seen that $S(.)$ is a function of only $\mathbf{s}$ and not r since P is a point in the far field. The first term in Eq. (6) represents the light reaching P after scattering at Q, whereas the second term represents light reaching the point P directly from the source without any scattering. The last two terms represent the interference of the scattered light with the unscattered light.

The CSD of a statistically stationary source of any state of coherence may be expanded as a linear combination of orthonormal functions $\phi_n(\mathbf{p},\omega)$ [26]:

$$W(\mathbf{p_1},\mathbf{p_2},\omega)=\sum_n\alpha_n(\omega)\phi_n^*(\mathbf{p_1},\omega)\phi_n(\mathbf{p_2},\omega), \tag{7}$$

where the functions $\phi_n(\mathbf{p},\omega)$ are the eigenfunctions and $\alpha_n(\omega)$ are the eigenvalues of the homogeneous Fredholm integral equation

$$\int_\sigma W(\mathbf{p_1},\mathbf{p_2},\omega)\phi_n(\mathbf{p_1},\omega)\mathrm{d}^2p_1=\alpha_n(\omega)\phi_n(p_2,\omega). \tag{8}$$

In other words, Eq. (7) states that CSD may be expressed as the sum of contributions from spatially completely coherent elementary sources if it is a continuous function and bounded throughout the source volume [26]. Substituting Eq. (7) into Eq. (6) we obtain an expression for the spectral density at a point P in the far field,

$$S(\mathbf{s},\omega)=\frac{|\Theta(\mathbf{r_i},\omega)|^2}{r_i^2}\sum_n\alpha_n(\omega)|\tilde{\phi}_n(k\mathbf{s}_{\mathbf{i}\perp},\omega)|^2+\sum_n\alpha_n(\omega)|\tilde{\phi}_n(k\mathbf{s}_\perp,\omega)|^2+\frac{e^{jkr_i}}{r_i}\Theta(\mathbf{r_i},\omega)e^{-jk\mathbf{s}\cdot\mathbf{r_i}}\sum_n\alpha_n(\omega)\tilde{\phi}_n(k\mathbf{s}_{\mathbf{i}\perp},\omega)\tilde{\phi}_n^*(k\mathbf{s}_\perp,\omega)+\frac{e^{-jkr_i}}{r_i}\Theta^*(\mathbf{r_i},\omega)e^{jk\mathbf{s}\cdot\mathbf{r_i}}\sum_n\alpha_n^*(\omega)\tilde{\phi}_n^*(k\mathbf{s}_{\mathbf{i}\perp},\omega)\tilde{\phi}_n(k\mathbf{s}_\perp,\omega), \tag{9}$$

where $\mathbf{s}_\perp$ and $\mathbf{s}_{\mathbf{i}\perp}$ are the projections of the vectors $\mathbf{s}$ and

$\mathbf{s_i}$ onto the $z=0$ plane and $\tilde{\phi}_n(.)$ is the spatial Fourier transform of $\phi_n(.)$ defined as

$$\tilde{\phi}_n(.,\omega) = \int \phi_n(\mathbf{p},\omega) e^{-j\mathbf{p}\cdot(.)} \mathrm{d}^2 p. \tag{10}$$

Taking a temporal Fourier transform of the spectral density gives us the intensity at the point P recorded as a hologram denoted by the function $H(.)$ and given by

$$H(\mathbf{s},\,.\,) = \int S(\mathbf{s},\omega) e^{-j\omega\cdot} \mathrm{d}\omega. \tag{11}$$

The first term in the expression for the hologram, obtained by substituting Eq. (9) into Eq. (11), is proportional to the intensity of the scattered light from the particle, and the second term is proportional to the reference beam without contribution from the object. Often the reference beam is recorded separately and subtracted from the hologram [7,9] to minimize the effects of the zero-order term. The third and the fourth terms result in the object image and a twin image of the object during reconstruction.

B. Numerical Reconstruction

The image of the object is formed by reconstructing the hologram numerically using the Helmholtz–Kirchhoff integral [7,9]. The reconstructed intensity at the point $\mathbf{r_c}$ in the reconstructed volume is given by

$$U(\mathbf{r_c},\tau) = \int_\Lambda H(\mathbf{s},\tau) e^{jk\mathbf{s}\cdot\mathbf{r_c}} \mathrm{d}^2 s_\perp. \tag{12}$$

The integral in the above equation runs over the area Λ of the detector plane. Hereafter, we focus our attention on the contribution of the third term in the expression for the hologram given by Eq. (11) [in conjunction with Eq. (9)]. This term results in the formation of an image of a point object located at $\mathbf{r_i}$ denoted as U_i and obtained by substituting the expression for the hologram in Eq. (12):

$$U_i(\mathbf{r_c},\tau) = \int \Theta(\mathbf{r_i},\omega) \frac{e^{jkr_i}}{r_i} \sum_n \alpha_n(\omega) \tilde{\phi}_n(k\mathbf{s}_{\mathbf{i}\perp},\omega) \times \int_\Lambda \tilde{\phi}_n{}^*(k\mathbf{s}_\perp,\omega) e^{jk\mathbf{s}\cdot(\mathbf{r_c}-\mathbf{r_i})} \mathrm{d}^2 s_\perp e^{-j\omega\tau} \mathrm{d}\omega. \tag{13}$$

Equation (13) describes the image formation in a DIHM with light of any state of coherence. It may be seen that the image formation for partially coherent light may be described in terms of the sum of contributions from completely spatially coherent modes,

$$U_i(\mathbf{r_c},\tau) = \sum_n U_i^n(\mathbf{r_c},\tau), \tag{14}$$

where

$$U_i^n(\mathbf{r_c},\tau) = \int \Theta(\mathbf{r_i},\omega) \frac{e^{jkr_i}}{r_i} \alpha_n(\omega) \tilde{\phi}_n(k\mathbf{s}_{\mathbf{i}\perp},\omega) \times \int_\Lambda \tilde{\phi}_n{}^*(k\mathbf{s}_\perp,\omega) e^{jk\mathbf{s}\cdot(\mathbf{r_c}-\mathbf{r_i})} \mathrm{d}^2 s_\perp e^{-j\omega\tau} \mathrm{d}\omega \tag{15}$$

is the contribution of the nth spatially coherent mode to the image formed. If the object is considered to be constituted of a collection of point objects in a volume Ω the image of such an object may be obtained by integrating Eq. (13) over all the object points in the volume Ω:

$$U(\mathbf{r_c},\tau) = \int_\Omega \int \Theta(\mathbf{r_i},\omega) \frac{e^{jkr_i}}{r_i} \sum_n \alpha_n(\omega) \tilde{\phi}_n(k\mathbf{s}_{\mathbf{i}\perp},\omega) \times \int_\Lambda \tilde{\phi}_n{}^*(k\mathbf{s}_\perp,\omega) e^{jk\mathbf{s}\cdot(\mathbf{r_c}-\mathbf{r_i})} \mathrm{d}^2 s_\perp e^{-j\omega\tau} \mathrm{d}\omega \mathrm{d}^3 r_i. \tag{16}$$

We may write Eq. (16) as

$$U(\mathbf{r_c},\tau) = \int_\Omega \int \Theta(\mathbf{r_i},\omega) \frac{e^{jkr_i}}{r_i} h_i(\mathbf{r_c}-\mathbf{r_i},\omega) e^{-j\omega\tau} \mathrm{d}\omega \mathrm{d}^3 r_i, \tag{17}$$

where $h_i(.,\omega)$ is the impulse response of the system given by

$$h_i(.,\omega) = \sum_n \alpha_n(\omega) \tilde{\phi}_n(k\mathbf{s}_{\mathbf{i}\perp},\omega) \int_\Lambda \tilde{\phi}_n{}^*(k\mathbf{s}_\perp,\omega) e^{jk\mathbf{s}\cdot(.)} \mathrm{d}^2 s_\perp. \tag{18}$$

It may be seen that the impulse response is a function of the position of the object through the term $\tilde{\phi}_n(k\mathbf{s}_{\mathbf{i}\perp},\omega)$, which makes the system shift variant for partially coherent light. We now proceed to discuss a few special cases.

C. Spatially Coherent Light

When the light is completely spatially coherent then the CSD may be represented by the lowest order mode ($n=0$). For this case, the impulse response is given by

$$h_i^{\mathrm{coh}}(.,\omega) = \alpha_0(\omega) \tilde{\phi}_0(k\mathbf{s}_{\mathbf{i}\perp},\omega) \int_\Lambda \tilde{\phi}_0{}^*(k\mathbf{s}_\perp,\omega) e^{jk\mathbf{s}\cdot(.)} \mathrm{d}^2 s_\perp. \tag{19}$$

D. Narrowband Light

For narrowband light the bandwidth $\Delta\omega$ is very small compared to center frequency ω_0. If the assumption that the modulus and the phase of the CSD function $W(.)$ is constant over $\Delta\omega$ is valid, then the CSD function may be approximated as $T(\omega)W(\mathbf{p_1},\mathbf{p_2},\omega_0)$, $T(\omega)$ being the spectral density of light. For this case the impulse response may be written as

$$h_i^{nb}(.,\omega) = T(\omega) \sum_n \alpha_n(\omega_0) \tilde{\phi}_n(k_0\mathbf{s}_{\mathbf{i}\perp},\omega_0) \times \int_\Lambda \tilde{\phi}_n{}^*(k_0\mathbf{s}_\perp,\omega_0) e^{jk_0\mathbf{s}\cdot(.)} \mathrm{d}^2 s_\perp. \tag{20}$$

E. Gaussian Schell Sources

A Schell model source is characterized by CSD of the form [25]

$$W(\mathbf{p_1},\mathbf{p_2},\omega)=\sqrt{S(\mathbf{p_1},\omega)}\sqrt{S(\mathbf{p_2},\omega)}\mu(\mathbf{p_1}-\mathbf{p_2},\omega), \quad (21)$$

where $S(\mathbf{p},\omega)$ is the spectral intensity at $\mathbf{p}$ and $\mu(\mathbf{p_1}-\mathbf{p_2},\omega)$ is the complex degree of spatial coherence. For the Gaussian Schell model sources the spectral intensity distribution and degree of coherence are Gaussian functions given by

$$S(\mathbf{p},\omega)=A(\omega)e^{-|\mathbf{p}|^2/2\sigma_s^2(\omega)}, \quad (22)$$

$$\mu(\mathbf{p_1}-\mathbf{p_2},\omega)=e^{-|\mathbf{p_1}-\mathbf{p_2}|^2/2\sigma_\mu^2(\omega)}. \quad (23)$$

For the Gaussian Schell model sources, the eigenfunctions and eigenvalues, $\phi_n(\mathbf{p},\omega)$ and $\lambda_n(\omega)$, that solve the Fredholm integral equation [Eq. (8)] are given by [27]

$$\phi_n(x)=\left(\frac{2c}{\pi}\right)^{1/4}\frac{1}{\sqrt{2^n n!}}H_n(x\sqrt{2c})e^{-cx^2}, \quad (24)$$

$$\alpha_n=A\left(\frac{\pi}{a+b+c}\right)\left(\frac{b}{a+b+c}\right)^n, \quad (25)$$

where $H_n(.)$ is a hermite polynomial of order n, $c=\sqrt{a^2+2ab}$, $a=1/4\sigma_s^2(\omega)$, and $b=1/2\sigma_\mu^2(\omega)$. In the above equations the dependence of a, b, and c on ω is dropped for convenience. The parameter β [27], defined as the ratio of σ_μ to σ_s, is the measure of degree of global coherence [27] of the source. When $\beta \gg 1$, the source may be said to be globally coherent and is well approximated by the lowest order mode. When $\beta \ll 1$ the source may be considered to be globally incoherent, and a larger number of modes of the order of $1/\beta$ are necessary to represent the source properly. The Fourier transform of $\phi_n(x)$ in Eq. (24) is given by

$$\tilde{\phi}_n(\nu)=\left(\frac{2c}{\pi}\right)^{1/4}\frac{1}{\sqrt{2^n n!}}\tilde{H}_n\left(\frac{\nu}{\sqrt{2c}}\right)e^{-\nu^2/4c}. \quad (26)$$

Substituting Eq. (26) into Eq. (20) we get the impulse response when a Gaussian Schell source with narrow temporal bandwidth centered at frequency ω_0 is used,

$$h_i^{\text{Schell}}(.,\omega)=T(\omega)\sum_n\left(\frac{2c}{\pi}\right)^{1/2}\frac{\alpha_n(\omega_0)}{2^n n!}\tilde{H}_n{}^*\left(\frac{k_0}{\sqrt{2c}}\mathbf{s_{i\perp}}\right)\times\int_\Lambda\tilde{H}_n\left(\frac{k_0}{\sqrt{2c}}\mathbf{s}_\perp\right)e^{-k_0^2(|\mathbf{s}_\perp|^2+|\mathbf{s}_{0\perp}|^2)/4c}e^{jk_0\mathbf{s}\cdot(.)}\mathrm{d}^2s_\perp. \quad (27)$$

One could express the impulse response in the time

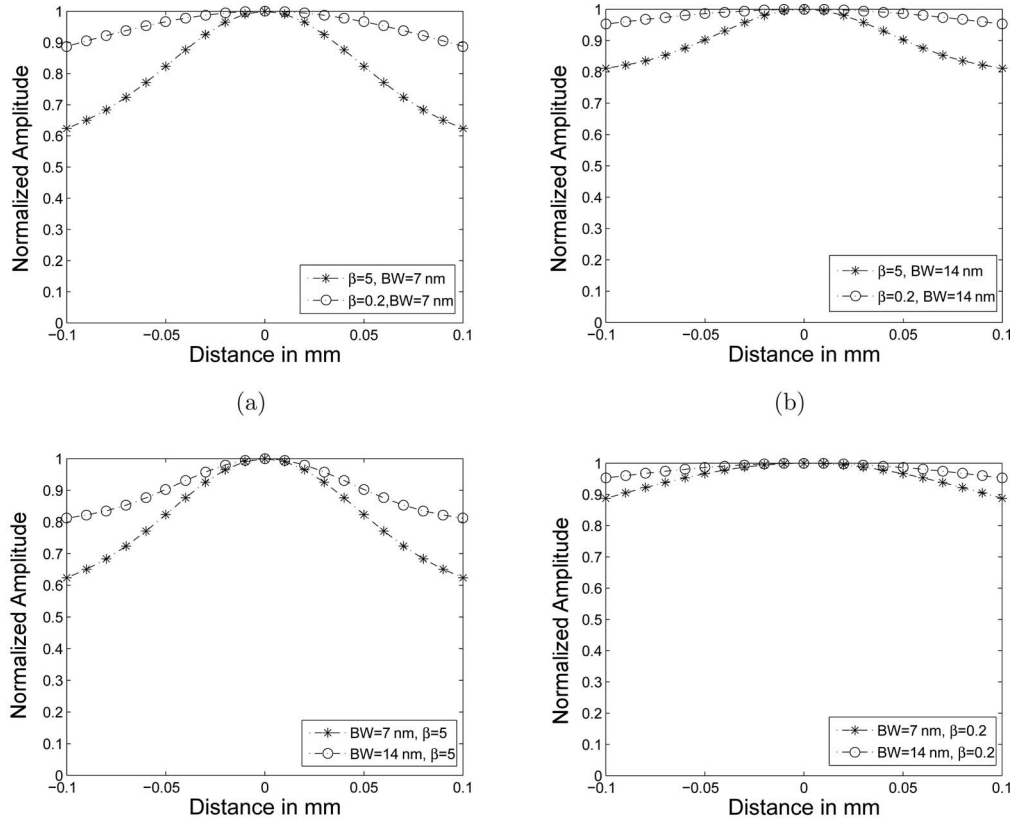

Fig. 2. Impulse response evaluated at $r_x=r_y=0$ for r_z ranging from −0.1 to 0.1 mm for a Gaussian Schell source with (a) $\beta=5$, $\beta=0.2$ and temporal FWHM bandwidth equal to 7 nm, (b) $\beta=5$, $\beta=0.2$ and temporal FWHM bandwidth equal to 14 nm, (c) temporal FWHM bandwidth equal to 7 and 14 nm with $\beta=5$, and (d) temporal FWHM bandwidth equal to 7 and 14 nm with $\beta=0.2$. The X axis in all four plots indicates distance Δ_{rz} in millimeters. The Y axis shows normalized amplitude.

domain by taking the temporal Fourier transform of Eq. (27).

$$h_i^{\text{Schell}}(.,\tau) = \psi(\tau)\sum_n \left(\frac{2c}{\pi}\right)^{1/2} \frac{\alpha_n(\omega_0)}{2^n n!} \tilde{H}_n^*\left(\frac{k_0}{\sqrt{2c}}\mathbf{s}_{i\perp}\right) \times \int_\Lambda \tilde{H}_n\left(\frac{k_0}{\sqrt{2c}}\mathbf{s}_\perp\right) e^{-k_0^2(|\mathbf{s}_\perp|^2+|\mathbf{s}_{0\perp}|^2)/4c} e^{jk_0\mathbf{s}\cdot(.)} \mathrm{d}^2 s_\perp, \tag{28}$$

where

$$\psi(\tau) = \int T(\omega) e^{j\omega\tau} \mathrm{d}\omega. \tag{29}$$

We simulate the impulse response of a DIHM as given in Eq. (28) (for $\mathbf{s}_{i\perp}=0$) when a narrowband Gaussian Schell model source is used. The distance D between the source and CCD was assumed to be 15 mm. The CCD was assumed to have a square pixel of width 6.7 μm. The temporal frequency distribution of the light $T(\omega)$ was assumed to have a Gaussian distribution with a center wavelength of 670 nm. The temporal coherence of the light is varied by varying the temporal bandwidth measured as full bandwidth at half wavelength (FBHW) of the Gaussian distribution. Figure 2 shows the plots of the absolute value of the impulse response $h(\mathbf{r})$ with the x and y the components of $\mathbf{r}$, r_x, and r_y equal to zero and r_z ranging from −0.1 to 0.1 mm in steps of 5 μm. In the plots shown in Figs. 2(a) and 2(b) the value of β is changed keeping the temporal coherence constant. As the value of β decreases from 5 to 0.2 (decreasing spatial coherence), the impulse response broadens in the Z direction. For $\beta=5$, the lowest order mode, $n=0$, was used to calculate the impulse response. For the other values of β, the first 21 modes ($n=0$ to 20) were used. In the plots shown in Figs. 2(c) and 2(d) the value of β is kept constant, and the temporal bandwidth of the light is changed. It may be observed that an increase in temporal bandwidth of the light (decreasing temporal coherence) results in the broadening of the impulse response. Figures 3(a)–3(d) show the corresponding plots of the absolute value of impulse response $h(\mathbf{r})$ when $r_z=0$. Again one observes a broadening of the impulse response in the $X-Y$ plane as the spatial and temporal coherence of light decreases.

3. EXPERIMENTS

A. System Description

The schematic of the setup used to study the effects of temporal and spatial coherence in a lensless digital inline holographic is shown in Fig. 4. Light from a primary source illuminates a spatial filter (SF) that serves as a secondary source. The objects used in this paper are spherical latex beads of 6 μm in diameter mounted onto a

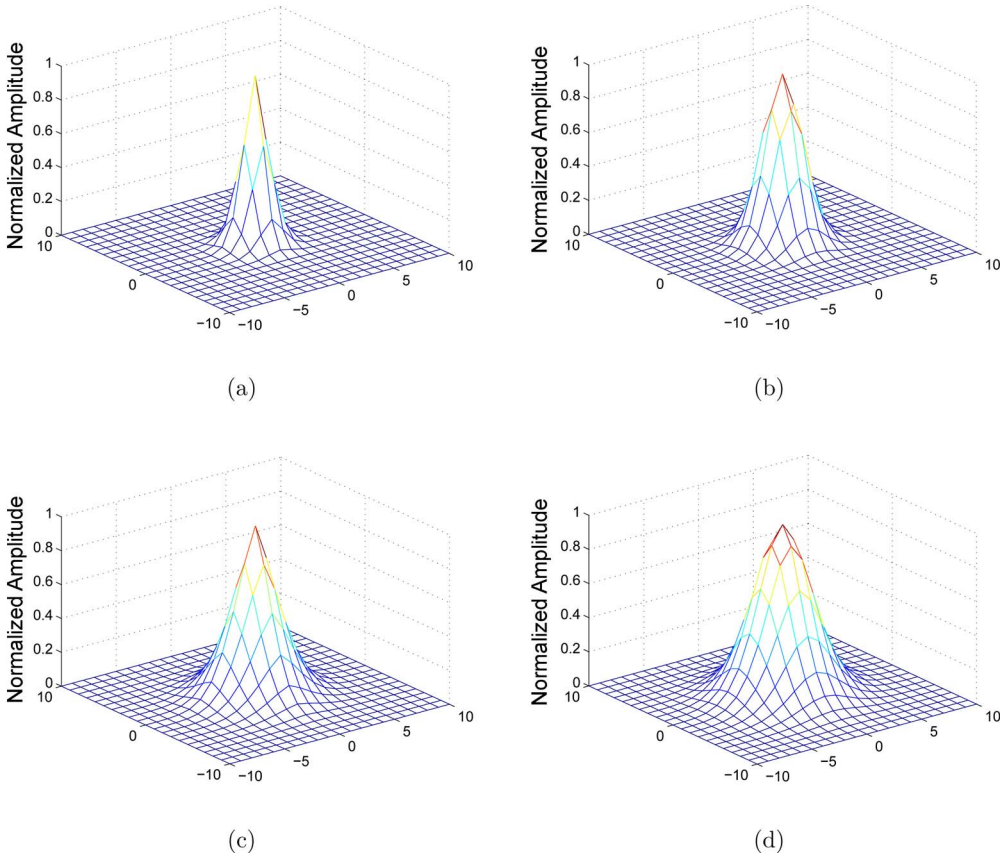

Fig. 3. (Color online) Impulse response evaluated in the plane $r_z=0$ for a Gaussian Schell source with (a) $\beta=5$, $\beta=0.2$ and temporal FWHM bandwidth equal to 7 nm, (b) $\beta=5$, $\beta=0.2$ and temporal FWHM bandwidth equal to 14 nm, (c) temporal FWHM bandwidth equal to 7 and 14 nm with $\beta=5$, and (d) temporal FWHM bandwidth equal to 7 and 14 nm with $\beta=0.2$. The X and Y axes in all four plots indicate r_x and r_y in pixels. Each pixel translates to a physical distance 3 μm. The Z axis shows normalized amplitude.

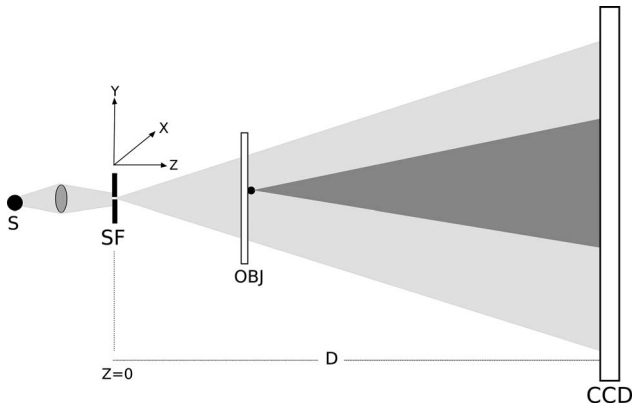

Fig. 4. Schematic of a lensless DIH setup. An SF, which acts as a secondary source, is illuminated via an imaging system by a primary source (S). The light scattered by the micro-object and the unscattered light forms an in-line hologram at the CCD plane.

microscopic slide. The light emanating from the pinhole is scattered by the object. The object beam interferes with the unscattered reference beam, and the hologram is recorded by a CCD (1000 pixels $\times$ 1000 pixels, pixel size 6.7 μm $\times$ 6.7 μm) placed at a distance 15 mm from the source. From each object hologram the zero-order term is removed by subtracting the reference wave intensity (recorded separately). The holograms are then used for the numerical reconstruction performed using Eq. (12) over volume $\Delta_x \times \Delta_y \times \Delta_z$ centered on the position of the object. The reconstruction space coordinates are given by $\mathbf{\Delta r} = \mathbf{r_c} - \mathbf{r_0}$ and has an origin at $\mathbf{r_c} = \mathbf{r_0}$. The resolution in the reconstructed volume is $\lambda D/N_x\delta_{dx}$ in the X direction and $\lambda D/N_y\delta_{dy}$ in the Y direction, where D is the distance between the source and the CCD, δ_{dx} and δ_{dy} are the pixel pitches of the CCD in the X and the Y directions, and N_x and N_y are the number of hologram pixels in the X and the Y directions.

B. Results and Discussion

Two light sources with different temporal coherence were used in the experiment. (1) LD1, a laser diode with center wavelength 670 nm and temporal full width at half-maximum (FWHM) bandwidth of 2 nm. (2) LD2, a laser diode with center wavelength 635 nm and FWHM bandwidth of 12 nm. The spatial coherence was varied by using spatial filters of two different diameters, 1 and 5 μm. As the diameter of the pinhole increases, the spatial coherence of light decreases. The light emanating from the pinhole can be considered to be spatially coherent if the absolute value of degree of coherence of light stays close to unity within the pinhole. If the degree of coherence of light drops considerably from the unity value within the pinhole, then the light is spatially incoherent. In light of the discussion in Section 2, partially spatially coherent

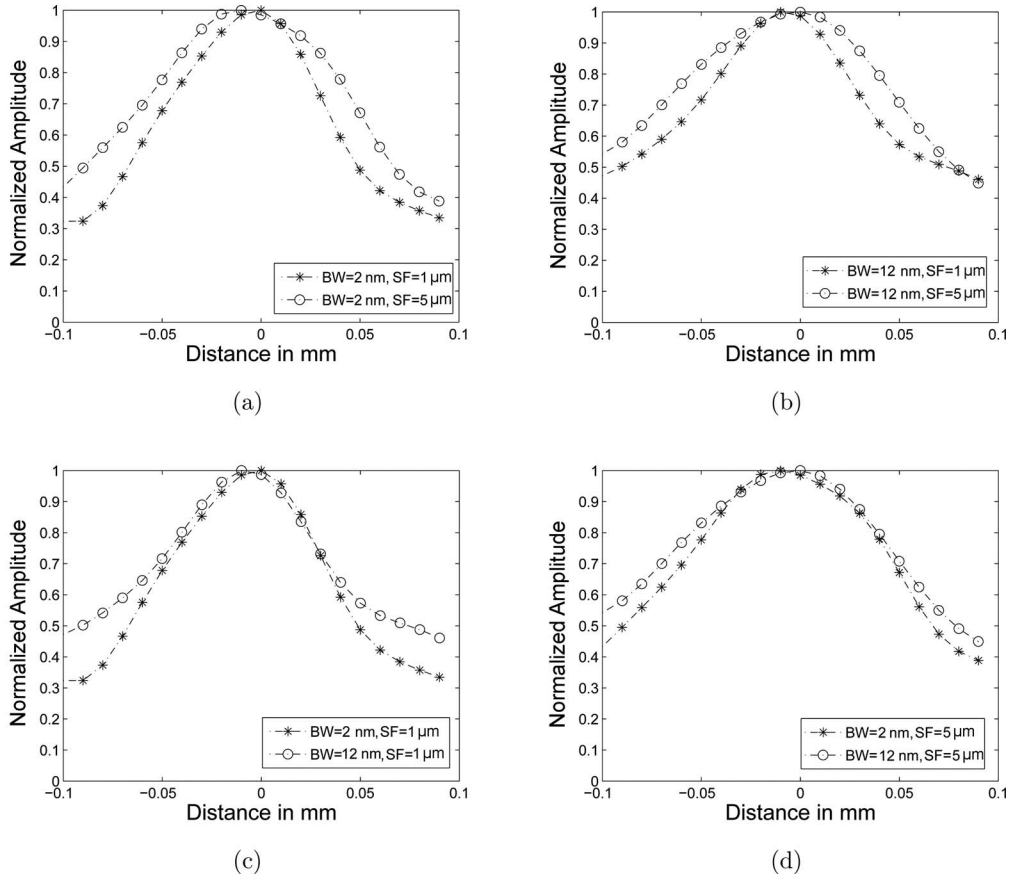

Fig. 5. Experimental result showing the reconstructed amplitude at $\Delta_{rx} = \Delta_{ry} = 0$ for Δ_{rz} ranging from -0.1 to 0.1 mm for (a) source LD1 (FWHM = 2 nm) with spatial filters of 1 and 5 μm in diameter, (b) source LD2 (FWHM = 12 nm) with spatial filters of 1 and 5 μm in diameter, (c) source LD1 and LD2 with spatial filter of 1 μm in diameter, and (d) source LD1 and LD2 with spatial filter of 5 μm in diameter. The X axis in all the four plots indicates distance Δ_{rz} in millimeters. The Y axis shows normalized amplitude.

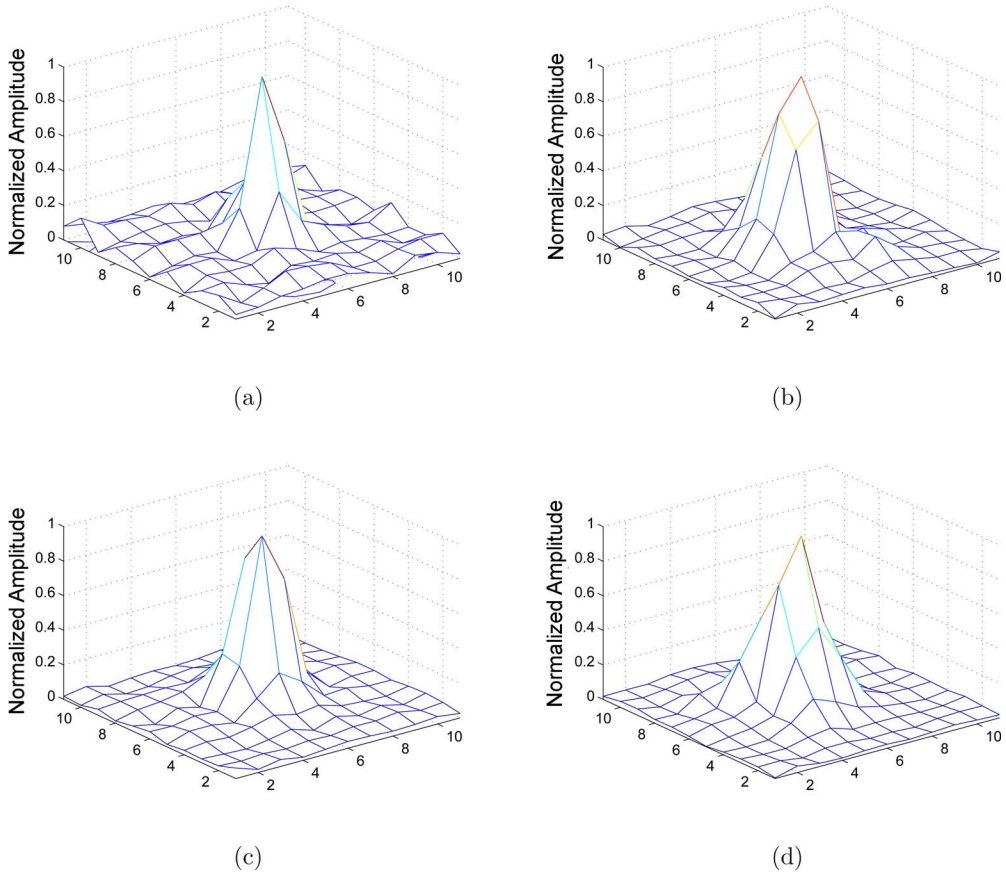

Fig. 6. (Color online) Experimental result showing the reconstructed amplitude in the plane $\Delta_{rz}=0$ for (a) source LD1 with spatial filter of 1 μm in diameter, (b) source LD1 with spatial filter of 5 μm in diameter, (c) source LD2 with spatial filter of 1 μm in diameter, and (d) source LD2 with spatial filter of 5 μm in diameter. The X and Y axes in all four plots indicate Δ_{rx} and Δ_{ry} in pixels. Each pixel corresponds to a distance of 3 μm in the reconstruction space. The Z axis shows normalized amplitude.

light can be described as the summation of a large number of spatially coherent modes. Shown in Figs. 5(a)–5(d) are plots of the reconstructed amplitude at $\Delta_{rx}=\Delta_{ry}=0$ for Δ_{rz} varying from −0.1 to 0.1 mm at intervals of 10 μm in the reconstruction space. Figure 5(a) shows plots when two different spatial filters of 1 and 5 μm in diameter are used with light source LD1. Figure 5(b) shows the corresponding plots for light source LD2. Figure 5(c) shows the plots when two light sources LD1 and LD2 are used with the spatial filter of 1 μm in diameter. Figure 5(d) shows the corresponding plots for the spatial filter of 5 μm in diameter. For a given temporal coherence of the light, as the spatial coherence decreases, the image of the bead is broader along the Z direction. Shown in Figs. 6(a)–6(d) are three-dimensional plots of the reconstructed amplitude in the plane $\Delta_{rz}=0$ of the reconstruction space. Given in Figs. 6(a) and 6(b) are the plots when the light source LD1 is used with spatial filters of 1 and 5 μm in diameter, respectively. Figures 6(c) and 6(d) are the corresponding plots for the light source LD2. It may be observed that a decrease in the spatial and temporal coherence of light leads to a broadening of the reconstructed image of beads.

4. CONCLUSION

We have theoretically analyzed the effects of partial coherence in a lensless DIH system. Our analysis is valid for primary or secondary sources of any state of coherence, though in this paper we have considered a planar secondary source. It was found that the impulse response of the system for light of any state of coherence is a function of the cross-spectral density of the light. The impulse response was simulated for the case of a Gaussian Schell model source. We have provided results from experiments used to image a spherical latex bead using a lensless DIH microscope using light from two different sources with varying temporal bandwidth in conjunction with spatial filters of two different sizes. The experimental results were found to be in general agreement with the predictions of theory and simulation.

ACKNOWLEDGMENTS

U. Gopinathan gratefully acknowledges the financial support of the Alexander Von Humboldt Foundation. This work was also supported by the German Science Foundation (DFG) grant OS. 111/19-2.

REFERENCES

1. D. Gabor, “A new microscopic principle,” Nature **161**, 777–778 (1948).
2. U. Schnars, H.-J. Hartman, and W. Jüptner, *Digital Holography* (Springer-Verlag, 2004).
3. J. J. Barton, “Removing multiple scattering and twin

images from holographic images," Phys. Rev. Lett. **67**, 3106–3109 (1991).
4. T. Latychevskaia and H.-W. Fink, "Solution to the twin image problem in holography," Phys. Rev. Lett. **98**, 233901 (2007).
5. G. Situ, J. P. Ryle, U. Gopinathan, and J. T. Sheridan, "Generalised in-line digital holographic technique based on intensity measurements at two different planes," Appl. Opt. **47**, 711–717 (2008).
6. M. Takeda, W. Wang, Z. Duan, and Y. Miyamoto, "Coherence holography," Opt. Express **13**, 9629–9635 (2005).
7. J. J. Barton, "Photoelectron holography," Phys. Rev. Lett. **61**, 1356–1359 (1988).
8. H.-W. Fink, W. Stocker, and H. Schmid, "Holography with low-energy electrons," Phys. Rev. Lett. **65**, 1204–1206 (1990).
9. J. Garcia-Sucerquia, W. Xu, S. K. Jericho, P. Klages, M. H. Jericho, and H. J. Kreuzer, "Digital in-line holographic microscopy," Appl. Opt. **45**, 836–850 (2006).
10. W. Xu, M. J. Jericho, I. A. Meinertzhagen, and H. J. Kreuzer, "Digital in-line holography of microspheres," Appl. Opt. **41**, 5367–5375 (2002).
11. W. Xu, M. J. Jericho, H. J. Kreuzer, and I. A. Meinertzhagen, "Tracking particles in four dimensions with in-line holographic microscopy," Opt. Lett. **28**, 164–166 (2003).
12. L. Repetto, E. Piano, and C. Pontiggia, "Lensless digital holographic microscope with light-emitting diode illumination," Opt. Commun. **29**, 1132–1134 (2004).
13. L. Repetto, R. Chittofrati, E. Piano, and C. Pontiggia, "Infrared lensless holographic microscope with a vidicon camera for inspection of metallic evaporations on silicon wafers," Opt. Commun. **251**, 44–50 (2005).
14. B. Javidi, I. Moon, S. Yeom, and E. Carapezza, "Three-dimensional imaging and recognition of microorganism using single-exposure on-line (SEOL) digital holography," Opt. Express **13**, 4492–4506 (2005).
15. S. Mayo, T. Davis, T. Gureyev, P. Miller, D. Paganin, A. Pogany, A. Stevenson, and S. Wilkins, "X-ray phase contrast microscopy and microtomography," Opt. Express **11**, 2289–2302 (2003).
16. D. Gao, S. W. Wilkins, D. J. Parry, T. E. Gureyev, P. R. Miller, and E. Hansen, "X-ray ultramicroscopy using integrated sample cells," Opt. Express **14**, 7889–7894 (2006).
17. G. Pedrini, F. Zhang, and W. Osten, "Digital holographic microscopy in the deep (193 nm) ultraviolet," Appl. Opt. **46**, 7829–7835 (2007).
18. J. Pomarico, U. Schnars, H.-J. Hartman, and W. Jüptner, "Digital recording and numerical reconstruction of holograms: a new method for displaying light in flight," Appl. Opt. **34**, 8095–8099 (1995).
19. G. Pedrini and H. J. Tiziani, "Short-coherence digital microscopy by use of a lensless holographic imaging system," Appl. Opt. **41**, 4489–4496 (2002).
20. L. Martínez-León, G. Pedrini, and W. Osten, "Applications of short-coherence digital holography in microscopy," Appl. Opt. **44**, 3977–3984 (2005).
21. T. Kozacki and R. Jóźwiki, "Near field hologram registration with partially coherent illumination," Opt. Commun. **237**, 235–242 (2004).
22. T. Kozacki and R. Jóźwiki, "Digital reconstruction of a hologram recorded using partially coherent illumination," Opt. Commun. **252**, 188–201 (2005).
23. J. Cheng and S. Han, "On x-ray in-line Gabor holography with a partially coherent source," Opt. Commun. **172**, 17–24 (1999).
24. L. Mandel and E. Wolf, *Optical Coherence and Quantum Optics* (Cambridge U. Press, 1995).
25. E. Wolf, *Introduction to the Theory of Coherence and Polarization of Light* (Cambridge U. Press, 2007).
26. E. Wolf, "New theory of partial coherence in the space-frequency domain. Part I: spectra and cross spectra of steady-state sources," J. Opt. Soc. Am. **72**, 343–351 (1982).
27. A. Starikov and E. Wolf, "Coherent-mode representation of Gaussian Schell-model sources and their radiation fields," J. Opt. Soc. Am. **72**, 923–928 (1982).